Nuclear Medicine and Biology 48 (2017) 1–8

Contents lists available at ScienceDirect

Nuclear Medicine and Biology

journal homepage: www.elsevier.com/locate/nucmedbio

Iminodiacetic acid as bifunctional linker for dimerization of cyclic RGD peptides

Dong Xu [a,1], Zuo-Quan Zhao [b,1], Shu-Ting Chen [c], Yong Yang [a,b], Wei Fang [b,*], Shuang Liu [d,**]

[a] International Medicine Center, International Medicine Division, Beijing Friendship Hospital, Capital Medical University, Beijing, China
[b] Department of Nuclear Medicine, Fuwai Hospital, the National Center for Cardiovascular Diseases, Chinese Academy of Medical Sciences and Peking Union Medical College, Beijing, China
[c] Key Laboratory of Radiopharmaceuticals, Ministry of Education, College of Chemistry, Beijing Normal University, Beijing, China
[d] School of Health Sciences, Purdue University, West Lafayette, IN, USA

ARTICLE INFO

Article history:
Received 11 October 2016
Received in revised form 3 January 2017
Accepted 17 January 2017
Available online xxxx

Keywords:
Integrin $\alpha_v\beta_3$
^{99m}Tc-labeling
Dimeric cyclic RGD peptides
Tumor imaging
SPECT

ABSTRACT

Introduction: In this study, I2P-RGD$_2$ was used as the example to illustrate a novel approach for dimerization of cyclic RGD peptides. The main objective of this study was to explore the impact of bifunctional linkers (glutamic acid vs. iminodiacetic acid) on tumor-targeting capability and excretion kinetics of the ^{99m}Tc-labeled dimeric cyclic RGD peptides.

Methods: HYNIC-I2P-RGD$_2$ was prepared by reacting I2P-RGD$_2$ with HYNIC-OSu in the presence of diisopropylethylamine, and was evaluated for its $\alpha_v\beta_3$ binding affinity against ^{125}I-echistatin bound to U87MG glioma cells. ^{99m}Tc-I2P-RGD$_2$ was prepared with high specific activity (~185 GBq/μmol). The athymic nude mice bearing U87MG glioma xenografts were used to evaluate its biodistribution properties and image quality in comparison with those of ^{99m}Tc-3P-RGD$_2$.

Results: The IC$_{50}$ value for HYNIC-I2P-RGD$_2$ was determined to be 39 ± 6 nM, which was very close to that (IC$_{50}$ = 33 ± 5 nM) of HYNIC-3P-RGD$_2$. Replacing glutamic acid with iminodiacetic acid had little impact on $\alpha_v\beta_3$ binding affinity of cyclic RGD peptides. ^{99m}Tc-I2P-RGD$_2$ and ^{99m}Tc-3P-RGD$_2$ shared similar tumor uptake values over the 2 h period, and its $\alpha_v\beta_3$-specificity was demonstrated by a blocking experiment. The uptake of ^{99m}Tc-I2P-RGD$_2$ was significantly lower than ^{99m}Tc-3P-RGD$_2$ in the liver and kidneys. The U87MG glioma tumors were visualized by SPECT with excellent contrast using both ^{99m}Tc-I2P-RGD$_2$ and ^{99m}Tc-3P-RGD$_2$.

Conclusion: Iminodiacetic acid is an excellent bifunctional linker for dimerization of cyclic RGD peptides. Bifunctional linkers have significant impact on the excretion kinetics of ^{99m}Tc radiotracers. Because of its lower liver uptake and better tumor/liver ratios, ^{99m}Tc-I2P-RGD$_2$ may have advantages over ^{99m}Tc-3P-RGD$_2$ for diagnosis of tumors in chest region.

1. Introduction

Integrin $\alpha_v\beta_3$ plays a significant role in tumor angiogenesis and metastasis [1–7]. It is a receptor for the extracellular matrix proteins (e.g., vitronectin, fibronectin, fibrinogen and laminin) with the exposed arginine–glycine–aspartic (RGD) tripeptide sequence [2,8–10]. It is expressed at low levels on epithelial cells and mature endothelial cells, but it is overexpressed on activated endothelial cells of neovasculature and tumor cells. The restricted $\alpha_v\beta_3$ expression during tumor growth and metastasis makes it an interesting target for development of $\alpha_v\beta_3$-targeted molecular imaging probes [11–20].

The RGD-containing cyclic pentapeptides (Fig. 1: c(RGDfK), RGD$_2$ (E[c(RGDfK)]$_2$); 2P-RGD$_2$ (E[PEG$_4$-c(RGDfK)]$_2$: PEG$_4$ = 15-amino-4,7,10,13-tetraoxapentadecanoic acid); and 3P-RGD$_2$ (PEG$_4$-E[PEG$_4$-

Abbreviations: ITLC, instant thin layer chromatography; MALDI, matrix-assisted laser desorption ionization; PET, positron emission tomography; RCP, radiochemical purity; SPECT, single photon emission computed tomography; HYNIC-OSu, sodium succinimidyl 6-(2-(2-sulfonatobenzaldehyde)hydrazono)-nicotinate); NOTA, 1,4,7-tritazacyclononane-1,4,7-triacetic acid; RGD$_2$: E[c(RGDfK)]$_2$, Glu[cyclo(Arg-Gly-Asp-D-Phe-Lys)]$_2$; RGD$_4$: E{E[c(RGDfK)]$_2$}$_2$, Glu{E[cyclo(Arg-Gly-Asp-D-Phe-Lys)]$_2$}$_2$; 2P-RGD$_2$: E[PEG$_4$-c(RGDfK)]$_2$, Glu[cyclo[Arg-Gly-Asp-D-Phe-Lys(PEG$_4$)]]$_2$ (PEG$_4$ = 15-amino-4,7,10,13-tetraoxapentadecanoic acid); 3P-RGD$_2$: PEG$_4$-E[PEG$_4$-c(RGKfD)]$_2$, PEG$_4$-Glu[cyclo[Arg-Gly-Asp-D-Phe-Lys(PEG$_4$)]]$_2$; I2P-RGD$_2$, *N*-(2-aminoethyl)iminodiacetyl-[cyclo[Arg-Gly-Asp-D-Phe-Lys(PEG$_4$)]]$_2$; HYNIC-3P-RGD$_2$, HYNIC-PEG$_4$-E[PEG$_4$-c(RGKfD)]$_2$ (HYNIC = 6-(2-(2-sulfonatobenzaldehyde)hydrazono)nicotinyl); HYNIC-I2P-RGD$_2$, HYNIC-*N*-(2-aminoethyl)iminodiacetyl-[cyclo[Arg-Gly-Asp-D-Phe-Lys(PEG$_4$)]]$_2$; ^{18}F-Alfatide-II, [^{18}F]AlF(NOTA-2P-RGD$_2$) (NOTA =1,4,7-tritazacyclononane-1,4,7-triacetic acid; ^{99m}Tc-3P-RGD$_2$, [^{99m}Tc(HYNIC-3P-RGD$_2$)(tricine)(TPPTS)] (TPPTS = trisodium triphenylphosphine-3,3′″,3″-trisulfonate); ^{99m}Tc-I2P-RGD$_2$, [^{99m}Tc(HYNIC-I2P-RGD$_2$)(tricine)(TPPTS)].

* Correspondence to: W. Fang, Department of Nuclear Medicine, Fuwai Hospital, the National Center for Cardiovascular Diseases, Chinese Academy of Medical Sciences and Peking Union Medical College, Beijing, China.
** Correspondence to: S. Liu, School of Health Sciences, Purdue University, 550 Stadium Mall Drive, West Lafayette, IN 47907, USA. Tel.: +1 765 494 0236; fax: +1 765 496 1377.
E-mail addresses: nuclearfw@126.com (W. Fang), liu100@purdue.edu (S. Liu).
[1] These authors contributed equally to this work.

http://dx.doi.org/10.1016/j.nucmedbio.2017.01.007
0969-8051/

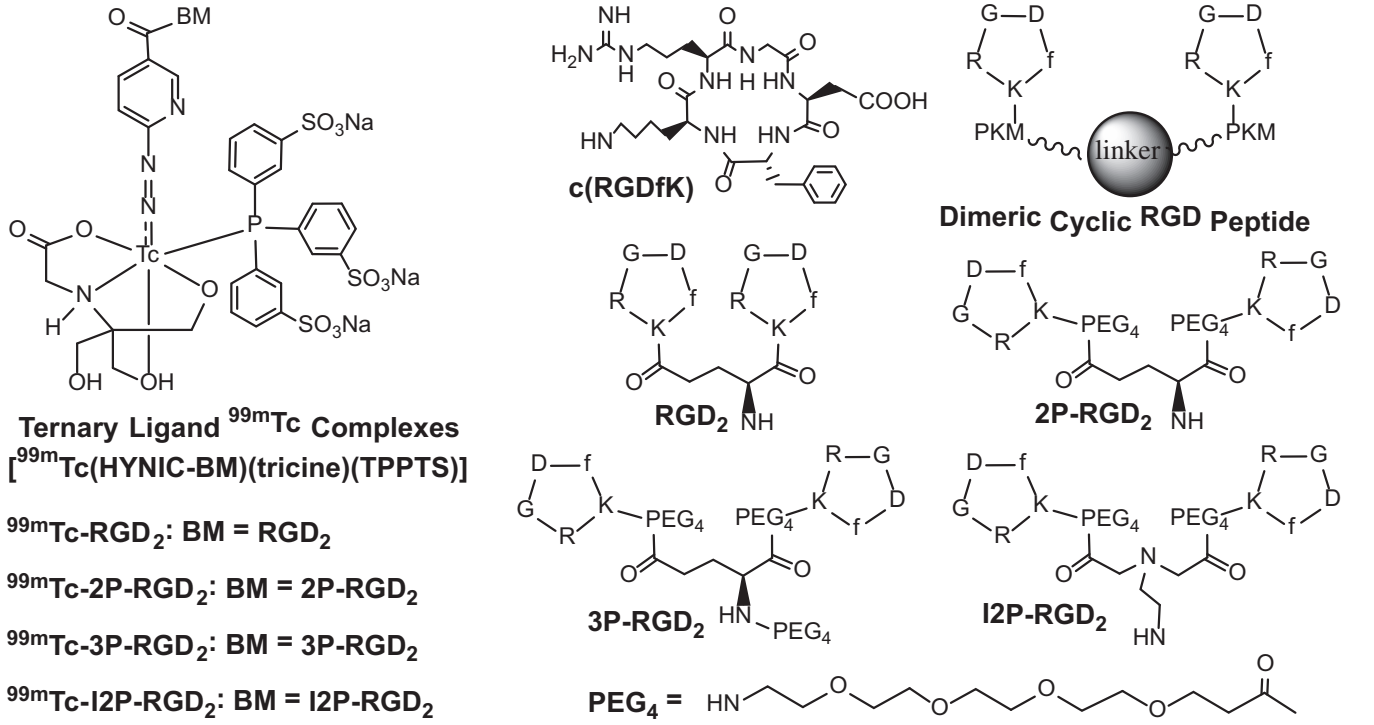

Fig. 1. The structures of dimeric cyclic RGD peptides (RGD_2, 2P-RGD_2, 3P-RGD_2 and I2P-RGD_2) and their ^{99m}Tc complexes [^{99m}Tc(HYNIC-BM)(tricine)(TPPTS)] (BM = biomolecule; ^{99m}Tc-RGD_2: BM = RGD_2; ^{99m}Tc-2P-RGD_2: BM = 2P-RGD_2; ^{99m}Tc-3P-RGD_2: BM = 3P-RGD_2; and ^{99m}Tc-I2P-RGD_2: BM = I2P-RGD_2). The RGD moiety is responsible for $\alpha_v\beta_3$-binding and tumor-targeting. PEG_4 groups are utilized to modify the excretion kinetics of ^{99m}Tc radiotracers from normal organs, and to keep the distance between two cyclic c(RGDfK) moieties in order to achieve bivalency. Glutamic and iminodiacetic acids are used as bifunctional linkers for dimerization of cyclic RGD peptides and attachment of the chelator, such as HYNIC.

c(RGDfK)$]_2$)) are potent $\alpha_v\beta_3$ antagonists [11,15,20]. We have been using dimeric, trimeric and tetrameric cyclic RGD peptides as targeting biomolecules (BM) to develop $\alpha_v\beta_3$-targeted radiotracers for tumor imaging by SPECT or PET [21–40]. Multiple cyclic RGD moieties are utilized to maximize the $\alpha_v\beta_3$-targeting capability and tumor uptake [11,15,20]. We found that radiolabeled (^{99m}Tc, ^{18}F, ^{64}Cu, ^{68}Ga and ^{111}In) multimeric cyclic RGD peptides all had higher tumor uptake with longer tumor retention time than their corresponding monomeric analogs [21–40], because of their higher $\alpha_v\beta_3$ binding affinity and their capability to target multiple integrins over-expressed in tumor tissues [20]. Among the dimeric cyclic RGD peptides evaluated in our laboratories, 2P-RGD_2 and 3P-RGD_2 show most promising results with respect to the tumor uptake and T/B ratios of their corresponding radiotracers [21–40]. Radiotracers ^{99m}Tc-3P-RGD_2 (Fig. 1: [^{99m}Tc(HYNIC-3P-RGD_2)(tricine)(TPPTS)]) and ^{18}F-Alfatide-II ([^{18}F]AlF(NOTA-2P-RGD_2)) are currently under clinical investigations as SPECT and PET radiotracers for tumor detection in cancer patients [41–49].

Dimeric cyclic RGD peptides are composed of two main components: c(RGDfK) moieties responsible for $\alpha_v\beta_3$-binding and a bifunctional linker (Fig. 1) for attachment of two c(RGDfK) moieties and conjugation of a chelator (e.g., HYNIC). Pharmacokinetic modifying groups (e.g., PEG_4 or Gly-Gly-Gly) are utilized to optimize the excretion kinetics of ^{99m}Tc radiotracers and to keep the distance between c(RGDfK) moieties in order to achieve bivalency. Over the last several years, we have been using glutamic acid for dimerization of cyclic RGD peptides [21–40]. In this study, we prepared a new dimeric cyclic RGD peptide conjugate HYNIC-2-(aminoethyl)iminodiacetyl-E[PEG_4-c(RGDfK)$]_2$ (HYNIC-I2P-RGD_2) using iminodiacetic acid as the bifunctional linker. Iminodiacetic acid is of our interest because it has similar length to glutamic acid. The $\alpha_v\beta_3$ binding affinity HYNIC-I2P-RGD_2 was determined in a displacement assay. ^{99m}Tc-I2P-RGD_2 ([^{99m}Tc(HYNIC-I2P-RGD_2)(tricine)(TPPTS)] (Fig. 1: ^{99m}Tc-I2P-RGD_2) was prepared and evaluated in athymic nude mice bearing U87MG glioma xenografts in comparison to ^{99m}Tc-3P-RGD_2. The main objectives of this study were to demonstrate the utility of iminodiacetic acid as a bifunctional linker for dimerization of cyclic RGD peptides, and explore the impact of bifunctional linkers (glutamic acid vs. iminodiacetic acid) on the tumor-targeting capability and excretion kinetics of their corresponding ^{99m}Tc radiotracer from normal organs (such as kidneys, liver and lungs).

2. Experimental section

2.1. Materials and instruments

Chemicals were purchased from Sigma/Aldrich (St. Louis, MO), and were used without further purification. The peptide *N*-(2-aminoethyl)iminodiacetyl-[cyclo[Arg-Gly-Asp-D-Phe-Lys(PEG_4)]]$_2$ (I2P-RGD_2) was custom-made by the Peptides International, Inc. (Louisville, KY). Sodium succinimidyl 6-(2-(2-sulfonatobenzaldehyde)hydrazono) nicotinate (HYNIC-OSu) was prepared according to literature method [50]. [^{99m}Tc(HYNIC-3P-RGD_2)(tricine)(TPPTS)] (^{99m}Tc-3P-RGD_2) was prepared using the procedure described in our previous reports [25]. $Na^{99m}TcO_4$ was obtained from Cardinal HealthCare (Chicago, IL). The MALDI (matrix-assisted laser desorption ionization) mass spectral data were collected on an Applied Biosystems Voyager DE PRO mass spectrometer (Framingham, MA), the Department of Chemistry, Purdue University.

2.2. HPLC methods

HPLC Method 1 used a LabAlliance HPLC system (Scientific Systems, Inc., State College, PA) equipped with a UV/vis detector (λ = 254 nm) and Zorbax C_{18} column (9.4 mm × 250 mm, 100 Å pore size; Agilent Technologies, Santa Clara, CA). The flow rate was 2.5 mL/min with a mobile phase being 90% A and 10% B at 0 min to 80%A and 20% B at 5 min, and to 50%A and 50% B at 20 min. The radio-HPLC (Method 2) used the LabAlliance HPLC system equipped with a β-ram IN/US detector

(Tampa, FL) and Zorbax C_{18} column (4.6 mm × 250 mm, 300 Å pore size; Agilent Technologies, Santa Clara, CA). The flow rate was 1 mL/min. The mobile phase was isocratic for the first 5 min with 90% A (25 mM NH_4OAc, pH = 6.8) and 10% B (acetonitrile), followed by a gradient mobile phase going from 90% A and 10% B at 5 min to 40% A and 60% B at 20 min.

2.3. Synthesis of HYNIC-I2P-RGD_2

HYNIC-OSu (13.5 mg, 30 μmol) and I2P-RGD_2 (5.9 mg, 3.2 μmol) were dissolved in anhydrous DMF (2 mL). After the addition of DIEA (5 drops), the mixture was stirred at room temperature for 24 h. To the reaction mixture was added 2 mL of water after completion of the reaction. The pH value was then adjusted to 3–4 using neat TFA. The product was separated from the reaction mixture by HPLC (Method 1). Fractions at ~15 min were collected. Lyophilization of collected fractions afforded the expected product HYNIC-I2P-RGD_2 as a white powder. The yield was 5.8 mg (~84%). MALDI-MS: $m/z = 2145.00$ for $[M + H]^+$ (M = 2145.28 calcd. For $[C_{95}H_{141}N_{25}O_{30}S]$).

2.4. Synthesis of ^{99m}Tc-I2P-RGD_2 and solution stability

To a lyophilized vial containing 20–25 μg HYNIC-I2P-RGD_2, 5 mg TPPTS, 6.5 mg tricine, 40 mg mannitol, 38.5 mg disodium succinate hexahydrate and 12.7 mg succinic acid was added 1.0–1.5 mL of $Na^{99m}TcO_4$ saline solution (~1110 MBq). The reconstituted vial was heated in a boiling water bath for 10–15 min, and then allowed to stand at room temperature for ~5 min. A sample of the resulting solution was analyzed by radio-HPLC (Method 2). The solution stability was monitored by HPLC for 6 h.

2.5. Dose preparation

For biodistribution, doses were prepared by dissolving ^{99m}Tc-I2P-RGD_2 in saline to a concentration of ~1 MBq/mL. For SPECT/CT imaging studies, doses were prepared by dissolving ^{99m}Tc-I2P-RGD_2 in saline to ~370 MBq/mL. In blocking experiment, RGD_2 was dissolved in the dose solution to 3.5 mg/mL. The resulting dose solution was filtered with a 0.20 μm Millex-LG filter before being injected into animals. Each animal was injected with ~0.1 mL of the dose solution.

2.6. Tumor cell culture

All human tumor cell lines (U87MG, MDA-MB-231, A549 and PC-3) were obtained from ATCC (Manassas, VA). U87MG glioma cells were cultured in the Minimum Essential Medium, Eagle with Earle's Balanced Salt Solution (non-essential amino acids sodium pyruvate). MDA-MB-231 human breast tumor cells were cultured in the RPMI Medium 1640 supplemented with 10% fetal bovine serum (FBS, ATCC). OVCAR-3 and PC-3 cancer cells were cultured in the F-12 medium (GIBCO, Grand Island, NY). All tumor cell lines were supplemented with 10% fetal bovine serum and 1% penicillin and streptomycin solution, and grown at 37 °C in a humidified atmosphere of 5% CO_2 in air. Cells were grown as monolayers and were harvested or split when they reached 90% confluence to maintain exponential growth.

2.7. In vitro whole-cell integrin $\alpha_v\beta_3$ binding assay

The integrin binding affinity was determined via a displacement assay using ^{125}I-echistatin (Perkin Elmer, Branford, CT) as the integrin-specific radioligand [35,29–40]. Briefly, the filter multiscreen DV plates (Millipore, Billerica, MA) were seeded with 1×10^5 U87MG cells in binding buffer (20 mM Tris, 150 mM NaCl, 2 mM $CaCl_2$, 1 mM $MnCl_2$, 1 mM $MgCl_2$, 0.1% (wt/vol) bovine serum albumin; and pH 7.4) and ^{125}I-echistatin (0.75–1.0 kBq) in the presence of increasing concentrations of the cyclic RGD peptide, incubated for 2 h at room temperature. After removing unbound ^{125}I-echistatin, the hydrophilic PVDF filters were washed three times with the binding buffer, and then collected. The radioactivity was determined using a PerkinElmer Wizard-1480 γ-counter (Shelton, CT). Experiments were carried out twice with triplicates. For comparison purpose, c(RGDyK), HYNIC-3P-RGD_2 and HYNIC-3P-RGD_2 were evaluated in the same assay. IC_{50} values were calculated by fitting experimental data with nonlinear regression using GraphPad Prism™ (GraphPad Software, Inc., San Diego, CA), and were reported as an average plus/minus standard deviation. Statistical analysis was performed by one-way analysis of variance (ANOVA). The level of significance was set at $p < 0.05$.

2.8. Animal models

Biodistribution and imaging studies were performed in compliance with the NIH animal experimentation guidelines (*Principles of Laboratory Animal Care*, NIH Publication No. 86-23, revised 1985). The animal protocol has been approved by the Institutional Animal Care and Use Committee of Purdue University (PACUC#: 1110000049) and Fuwai Hospital (Chinese Academy of Medical Sciences and Peking Union Medical College). Female athymic *nu/nu* mice (4–5 weeks) were purchased from Harlan (Indianapolis, IN), and were inoculated subcutaneously with tumor cells into the shoulder flank (5×10^6 of U87MG cells) or left/right mammary fat pad (1×10^6 MDA-MB-231, OVAR-3 of PC-3) of each animal. Four to six weeks after inoculation, the tumor size was 0.1–0.5 g, and animals were used for biodistribution and imaging studies. All procedures were performed in a laminar flow cabinet under aseptic conditions.

2.9. Biodistribution protocol

The tumor-bearing mice ($n = 5$; 20–25 g) were randomly selected, and each animal was administered with ~0.1 MBq of ^{99m}Tc-I2P-RGD_2 by tail vein injection. Animals were sacrificed by sodium pentobarbital overdose (~200 mg/kg) at 5, 30, 60 and 120 min p.i. Blood, tumors and normal organs (brain, eyes, heart, spleen, lungs, liver, kidneys, muscle and intestine) were harvested, washed with saline, dried with absorbent tissue, weighed, and counted on a PerkinElmer Wizard-1480 γ-counter (Shelton, CT). The organ uptake was calculated as the percentage of injected dose (%ID) or the percentage of injected dose per gram of wet tissue (%ID/g). The blocking experiment was performed using RGD_2 as the blocking agent in four animals. Each animal was administered with ~0.1 MBq of ^{99m}Tc-I2P-RGD_2 along with ~350 μg (~14 mg/kg) of RGD_2. Biodistribution data (%ID/g) and tumor-to-background (T/B) ratios were expressed as the average plus standard deviation on the basis of the results from 5 to 8 animals in each group. Statistical analysis was performed by one-way analysis of variance (ANOVA). The level of significance was set at $p < 0.05$.

2.10. SPECT/CT imaging

SPECT/CT images were obtained for the athymic nude mice ($n = 2$ for each tumor type) bearing U87MG, MDA-MB-231, OVCAR-3 and PC-3 xenografts using a u-SPECT-II/CT scanner (Milabs, the Netherlands) equipped with a 0.6 mm multi-pinhole collimator. The animal was injected with ~37 MBq of ^{99m}Tc-I2P-RGD_2 in 0.1 mL saline via the tail vein. At 60 min p.i., the animal was placed into a shielded chamber connected to an isoflurane anesthesia unit (Univentor, Zejtun, Malta). Anesthesia was induced using an air flow rate of 350 mL/min and ~3.0% isoflurane. After induction of anesthesia, the animal was placed supine on the scanning bed. The air flow rate was then reduced to ~250 mL/min with ~2.0% isoflurane. Rectangular scan in the regions of interest (ROIs) from SPECT and CT were selected on the basis of orthogonal optical images provided by the integrated webcams. After SPECT (75 projections over 30 min per frame, 2 frames), the animal was transferred into the attached CT scanner and imaged using the

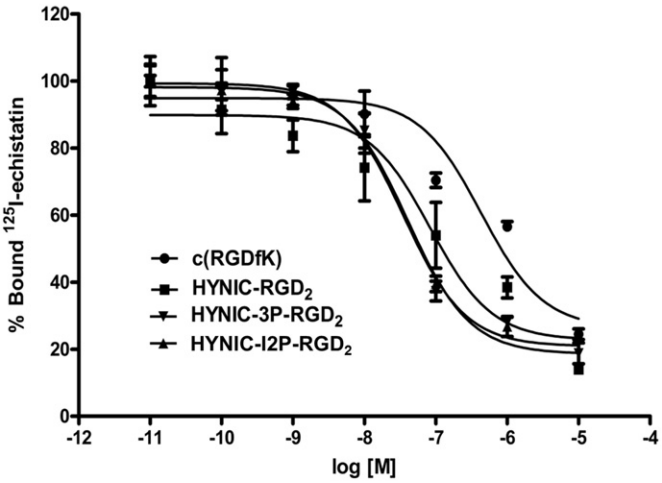

Fig. 2. The displacement curves of ^{125}I-echistatin bound to U87MG human glioma cells in the presence of cyclic RGD peptides. c(RGDfK) was the "control" to validate the assay. HYNIC-RGD_2 and HYNIC-3P-RGD_2 were used for comparison purpose. IC_{50} values were calculated to be 32 ± 5, 39 ± 6, 85 ± 8, and 422 ± 15 nM for HYNIC-3P-RGD_2, HYNIC-I2P-RGD_2, HYNIC-RGD_2 and c(RGDfK), respectively.

'normal' acquisition settings (2 degree intervals) at 45 kV and 500 μA. After CT acquisition, the animal was allowed to recover in a lead-shielded cage.

2.11. Image reconstruction and data processing

Reconstruction was performed using a POSEM (pixelated ordered subsets by expectation maximization) algorithm with 6 iterations and 16 subsets. CT data were reconstructed using a cone-beam filtered back-projection algorithm (NRecon v1.6.3, Skyscan). After reconstruction, the SPECT and CT data were co-registered according to the movement of the robotic stage, and re-sampled to equivalent voxel sizes. The co-registered images were visualized using the PMOD software (PMOD Technologies, Zurich, Switzerland). A 3D-Guassian filter (0.8 mm FWHM) was applied to smooth noise, and the LUTs (look up tables) were adjusted for good contrast. The reconstructed images were visualized as both orthogonal slices and maximum intensity projections.

2.12. Immunohistochemistry

The xenografted tumor tissues (U87MG, MDA-MB-231, OVAR-3 and PC-3) were harvested, snap-frozen in the OCT (optimal cutting temperature compound) solution, and cut into slices (5 μm). After drying thoroughly, the slides were fixed with ice-cold acetone for 10 min, and dried in air for 20 min. Sections were blocked with 10% goat serum for 30 min, and then were incubated with the hamster anti-integrin β_3 antibody (1:100, BD Biosciences, San Jose, CA) and rat anti-CD31 antibody (1:100, BD Biosciences, San Jose, CA) for 1 h at room temperature. After incubating with Cy3-conjugated goat anti-hamster and FITC-conjugated goat anti-rat secondary antibodies (1:100, Jackson ImmunoResearch Inc., West Grove, PA) and washing with PBS. The fluorescence was visualized with an Olympic BX51 microscope (Olympus America Inc., Center Valley, PA). All pictures were taken under 200× magnification using the same exposure time. The average area of positively stained CD31 or β_3 on cryostat sections from >15 randomly selected fields in each group was calculated to assess the relative β_3 expression in tumor tissues by the NIH *ImageJ* software. The fluorescent density data were expressed as a percentage of the total area, presented as the mean ± S.D., and plotted against the tumor uptake of ^{99m}Tc-I2P-RGD_2. Experiments were performed three times. Statistical analysis was performed by Newman–Keuls multiple comparison. The level of significance was set at $p < 0.05$.

Table 1
Selected biodistribution data and tumor-to-background ratios of ^{99m}Tc-I2P-RGD_2 in athymic nude mice ($n = 5$) bearing U87MG human glioma xenografts.

Organ	5 min	30 min	60 min	120 min
Blood	3.62 ± 0.41	1.02 ± 0.04	0.51 ± 0.05	0.27 ± 0.04
Brain	0.34 ± 0.10	0.30 ± 0.06	0.16 ± 0.02	0.18 ± 0.06
Eyes	2.48 ± 0.63	3.46 ± 0.92	2.25 ± 1.11	1.96 ± 0.72
Heart	4.30 ± 0.91	3.21 ± 0.80	1.82 ± 0.39	1.51 ± 0.43
Intestine	23.99 ± 5.72	12.32 ± 2.89	7.36 ± 1.34	7.11 ± 0.84
Kidney	24.80 ± 3.83	16.07 ± 1.43	12.17 ± 1.16	9.73 ± 1.37
Liver	5.55 ± 0.49	2.45 ± 0.19	1.76 ± 0.21	1.67 ± 0.40
Lungs	6.44 ± 1.21	4.55 ± 0.48	2.28 ± 0.45	2.27 ± 0.27
Muscle	2.46 ± 0.50	2.19 ± 0.28	1.39 ± 0.34	1.21 ± 0.36
Spleen	5.03 ± 0.65	3.26 ± 0.62	2.91 ± 0.70	2.69 ± 0.53
Tumor	7.24 ± 1.18	6.61 ± 0.88	5.61 ± 1.38	5.28 ± 1.31
Tumor/Blood	2.04 ± 0.29	6.48 ± 0.72	9.31 ± 0.44	22.35 ± 4.51
Tumor/Liver	1.32 ± 0.28	2.68 ± 0.59	2.85 ± 0.33	3.47 ± 0.75
Tumor/Lung	1.08 ± 0.12	1.44 ± 0.20	2.13 ± 0.30	2.34 ± 0.41
Tumor/Muscle	3.13 ± 0.51	3.10 ± 0.26	3.33 ± 0.52	3.82 ± 0.15

The tumor uptake was expressed as an average plus/minus the standard deviation.

Table 2
Selected biodistribution data and tumor-to-background ratios of ^{99m}Tc-3P-RGD_2 in athymic nude mice ($n = 5$) bearing U87MG human glioma xenografts.

Organ	5 min	30 min	60 min	120 min
Blood	3.47 ± 0.35	1.01 ± 0.10	0.70 ± 0.11	0.35 ± 0.01
Brain	0.33 ± 0.08	0.17 ± 0.02	0.16 ± 0.02	0.14 ± 0.04
Eyes	2.67 ± 0.56	2.18 ± 0.57	2.00 ± 0.28	1.52 ± 0.04
Heart	5.10 ± 0.77	3.83 ± 0.64	2.01 ± 0.19	1.38 ± 0.07
Intestine	4.93 ± 0.48	5.53 ± 0.65	4.98 ± 0.21	3.47 ± 0.71
Kidney	37.24 ± 2.90	28.44 ± 0.98	20.39 ± 0.90	16.28 ± 0.87
Liver	9.25 ± 0.76	5.45 ± 0.12	4.68 ± 0.40	4.50 ± 0.42
Lungs	7.17 ± 0.98	4.54 ± 0.19	3.41 ± 0.57	2.31 ± 0.25
Muscle	3.43 ± 0.21	2.78 ± 1.37	1.73 ± 0.25	1.44 ± 0.03
Spleen	5.52 ± 1.12	4.98 ± 0.17	3.64 ± 0.34	3.69 ± 0.39
Tumor	4.98 ± 1.29	5.51 ± 0.80	4.68 ± 0.61	4.11 ± 0.67
Tumor/Blood	1.43 ± 0.85	5.41 ± 0.21	6.68 ± 1.21	11.74 ± 2.71
Tumor/Liver	0.53 ± 0.02	1.01 ± 0.45	1.01 ± 0.45	0.91 ± 0.75
Tumor/Lung	0.69 ± 0.12	1.21 ± 0.47	1.37 ± 0.25	1.77 ± 0.86
Tumor/Muscle	1.45 ± 0.77	1.98 ± 1.12	2.70 ± 0.89	2.85 ± 0.45

The tumor uptake was expressed as an average plus/minus the standard deviation.

3. Results

3.1. Synthesis of HYNIC-I2P-RGD_3

HYNIC-I2P-RGD_2 was prepared from the reaction of I2P-RGD_2 with excess HYNIC-OSu in the presence of DIEA. It took ~24 h to complete the conjugation reaction at room temperature. HYNIC-I2P-RGD_2 was purified by HPLC and characterized by ESI-MS. Its HPLC purity was >95% before being used for the in vitro $\alpha_v\beta_3$ binding assay and ^{99m}Tc-labeling. ESI-MS data were consistent with the proposed composition for HYNIC-I2P-RGD_2.

3.2. Integrin $\alpha_v\beta_3$ binding affinity

The $\alpha_v\beta_3$ binding affinity of HYNIC-I2P-RGD_2 was determined using an in vitro displacement assay. Fig. 2 shows the displacement curves of ^{125}I-echistatin bound to U87MG glioma cells in the presence of cyclic RGD peptides. IC_{50} values were calculated to be 33 ± 5, 39 ± 6, 85 ± 5 and 422 ± 45 nM for HYNIC-3P-RGD_2, HYNIC-I2P-RGD_2, HYNIC-RGD_2 and c(RGDyK), respectively. The $\alpha_v\beta_3$ binding affinity follows the order of HYNIC-3P-RGD_2 ~ HYNIC-I2P-RGD_2 > HYNIC-RGD_2 > > c(RGDyK). These results are completely consistent with those from our previous studies [29–32,36–38]. HYNIC-I2P-RGD_2 has the IC_{50} value (IC_{50} = 39 ± 6 nM) almost identical to that of HYNIC-3P-RGD_2 (IC_{50} = 33 ± 5 nM). Replacing glutamic acid in HYNIC-3P-RGD_2 with the iminodiacetyl linker had little impact on the $\alpha_v\beta_3$ binding

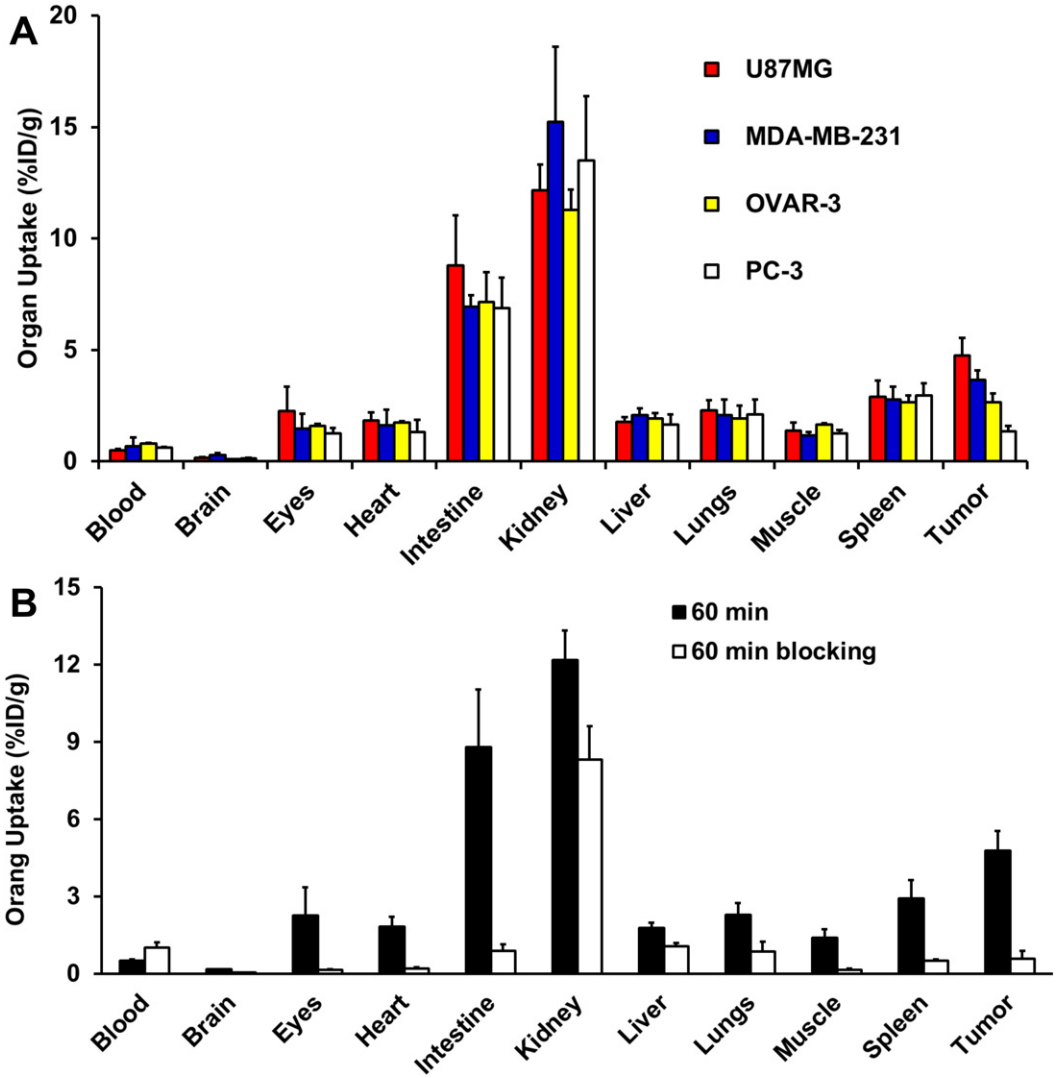

Fig. 3. A: Comparison of the 60-min biodistribution data of ^{99m}Tc-I2P-RGD$_2$ ($n = 5$) in the athymic nude mice bearing U87MG, MDA-MB-231, OVAR-3 and PC-3 xenografts. Its uptake in normal organs was almost identical, but its uptake values were significantly different in 4 xenografted tumors (U87MG, MDA-MB-231, OVAR-3 and PC-3 xenografts). This experiment was designed to demonstrate the dependence of its tumor uptake on integrin $\alpha_v\beta_3$ expression levels in xenografted tumor tissues. B: The selected 60-min biodistribution data of ^{99m}Tc-I2P-RGD$_2$ in athymic nude mice ($n = 5$) bearing U87MG glioma xenografts with/without co-injection of RGD$_2$ (350 μg/mouse or 14 mg/kg). The blocking experiment was designed to demonstrate its integrin $\alpha_v\beta_3$ specificity.

affinity of dimeric cyclic RGD peptides, as long as the distance between the two cyclic RGD moieties is long enough.

3.3. Radiochemistry

^{99m}Tc-I2P-RGD$_2$ was prepared from the reaction of HYNIC-I2P-RGD$_2$ with $^{99m}TcO_4^-$ in the presence of excess tricine and TPPTS using a kit formulation. ^{99m}Tc-labeling was accomplished by heating the reaction mixture at 100 °C for 10–15 min. Its RCP was always >95% without post-labeling chromatographic purification, and remained stable for >6 h in the kit matrix (Fig. SI1). The specific activity was very high (~185 GBq/μmol).

3.4. Biodistribution properties

Biodistribution was performed on ^{99m}Tc-I2P-RGD$_2$ and ^{99m}Tc-3P-RGD$_2$ (positive control) in the athymic nude mice bearing U87MG glioma xenografts. Their biodistribution data are listed in Tables 1 and 2, respectively. We found that ^{99m}Tc-I2P-RGD$_2$ and ^{99m}Tc-3P-RGD$_2$ shared almost identical tumor uptake values over the 2 h study period. Even though the tumor uptake of ^{99m}Tc-I2P-RGD$_2$ (7.24 ± 1.18%ID/g) was slightly higher than that of ^{99m}Tc-3P-RGD$_2$ (4.98 ± 1.29%ID/g) at 5 min p.i., this difference was not significant within the experimental error. ^{99m}Tc-I2P-RGD$_2$ and ^{99m}Tc-3P-RGD$_2$ also shared similar lung uptake values. However, the liver uptake of ^{99m}Tc-I2P-RGD$_2$ (5.55 ± 0.49, 2.45 ± 0.19, 1.76 ± 0.21 and 1.67 ± 0.40%ID/g at 5, 30, 60, and 120 min p.i., respectively) was significantly lower than ^{99m}Tc-3P-RGD$_2$ (9.25 ± 0.76, 5.45 ± 0.12, 4.68 ± 0.40 and 4.50 ± 0.42%ID/g at 5, 30, 60, and 120 min p.i., respectively). As a result, the tumor/liver ratios for ^{99m}Tc-I2P-RGD$_2$ were much better than those of ^{99m}Tc-3P-RGD$_2$ over the 2 h period (Tables 1 and 2). ^{99m}Tc-I2P-RGD$_2$ also had lower kidney uptake than ^{99m}Tc-3P-RGD$_2$. The intestine uptake of ^{99m}Tc-I2P-RGD$_2$ was much higher than those of ^{99m}Tc-3P-RGD$_2$ (Tables 1 and 2). We also compared the biodistribution properties of ^{99m}Tc-I2P-RGD$_2$ in three other tumor-bearing models (Fig. 3A: MDA-MB-231, OVAR-3 and PC-3). It was found that the uptake values of ^{99m}Tc-I2P-RGD$_2$ in normal organs of the four different tumor-bearing athymic nude mice were almost identical within experimental error, but its tumor uptake values were different depending on the tumor types (Fig. 3A: U87MG: 5.61 ± 1.38%ID/g; MDA-MB-231: 3.67 ± 0.42%ID/g; OVAR-3: 2.65 ± 0.40%ID/g; and PC-3 1.35 ± 0.24%ID/g). Similar trend was also seen with ^{99m}Tc-3P-RGD$_2$ in the same tumor-bearing models [30,35,36].

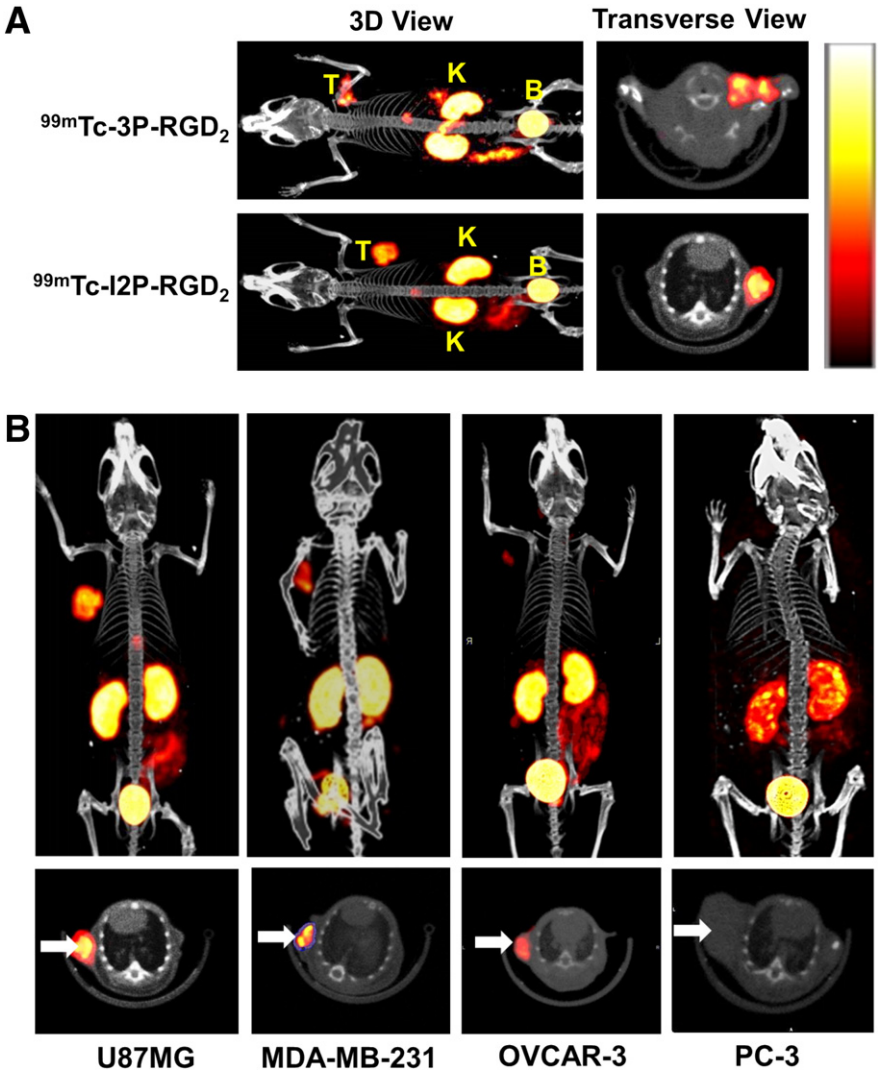

Fig. 4. A: The 3D and transverse views of SPECT/CT images of the athymic nude mice (B = bladder; I = intestine; K = kidney and T = tumor) bearing U87MG human glioma xenografts. Each animal was administered with ~37 MBq of ^{99m}Tc-I2P-RGD$_2$ or ^{99m}Tc-3P-RGD$_2$. B: The 3D and transverse views of SPECT/CT images of athymic nude mice ($n = 2$ for each tumor type) bearing U87MG, MDA-MB-231, OVCAR-3 or PC-3 xenografts. Each animal was administered with ~55 MBq of ^{99m}Tc-I2P-RGD$_2$ via tail-vein. The radioactivity in the intestines was quite obvious in all animals.

3.5. Integrin $\alpha_v\beta_3$ specificity

A blocking experiment was performed to demonstrate the $\alpha_v\beta_3$ specificity of ^{99m}Tc-I2P-RGD$_2$ using RGD$_2$ as the blocking agent (350 μg/mouse or 14 mg/kg) since it is a well-established $\alpha_v\beta_3$ antagonist [16]. Fig. 3B shows the 60-min biodistribution data of ^{99m}Tc-I2P-RGD$_2$ in the athymic nude mice ($n = 5$) bearing U87MG glioma xenografts in the absence/presence of excess RGD$_2$. We found that co-injection of excess RGD$_2$ significantly blocked the tumor uptake of ^{99m}Tc-I2P-RGD$_2$ (0.59 ± 0.28%ID/g with RGD$_2$ vs. 5.61 ± 1.38%ID/g without RGD$_2$). The normal organ uptake was also blocked significantly by co-injection of RGD$_2$. For example, the uptake of ^{99m}Tc-I2P-RGD$_2$ in the intestine, lungs and spleen was 7.36 ± 1.34, 2.28 ± 0.45, and 2.91 ± 0.71%ID/g, respectively, without RGD$_2$. Its uptake in the same organs was 0.88 ± 0.26, 0.85 ± 0.39, and 0.51 ± 0.03%ID/g, respectively, in the presence of excess RGD$_2$. The results from this experiment clearly showed that the tumor uptake of ^{99m}Tc-I2P-RGD$_2$ is $\alpha_v\beta_3$-specific. Similar conclusion was also made for other radiolabeled (^{99m}Tc and ^{111}In) dimeric cyclic RGD peptides [36–40].

3.6. SPECT/CT

Fig. 4A shows the representative 3D and transverse views of SPECT/CT images of the U87MG glioma-bearing mice administered with ~37 MBq of ^{99m}Tc-I2P-RGD$_2$ and ^{99m}Tc-3P-RGD$_2$, respectively. The U87MG glioma tumors were clearly visualized by SPECT with excellent contrast. High uptake in the intestines and kidneys was also seen in the SPECT images of the glioma-bearing mice. These results clearly demonstrated that ^{99m}Tc-I2P-RGD$_2$ is as good as ^{99m}Tc-3P-RGD$_2$ as the $\alpha_v\beta_3$-targeted radiotracer for tumor imaging. We also obtained SPECT/CT images of the athymic nude mice bearing MDA-MB-231, OVAR-3 and PC-3 tumor xenografts (Fig. 4B). We found that the tumor uptake of ^{99m}Tc-I2P-RGD$_2$ followed the general ranking order of U87MG > MDA-MB-231 > OVAR-3 > PC-3. The xenografted U87MG glioma tumors had the highest uptake with the best contrast. The xenografted PC-3 tumor was not clearly visualized due to its low $\alpha_v\beta_3$ expression (Fig. SI2). The tumor/background contrast for MDA-MB-231 and OVAR-3 tumors was not as good as that of U87MG gliomas; but it was much better than that of PC-3 tumors. These results suggest that ^{99m}Tc-I2P-RGD$_2$ may have the utility for noninvasive measurement of the relative $\alpha_v\beta_3$ expression levels in tumors of different origin.

3.7. Relationship between $\alpha_v\beta_3$ expression level and tumor uptake

Fig. SI2 shows microscopic fluorescence images of the xenografted tumor tissues (U87MG, MDA-MB-231, OVAR-3 and PC-3) labeled with anti-integrin β_3 (red) and anti-CD31 (green) antibodies. In the overlay

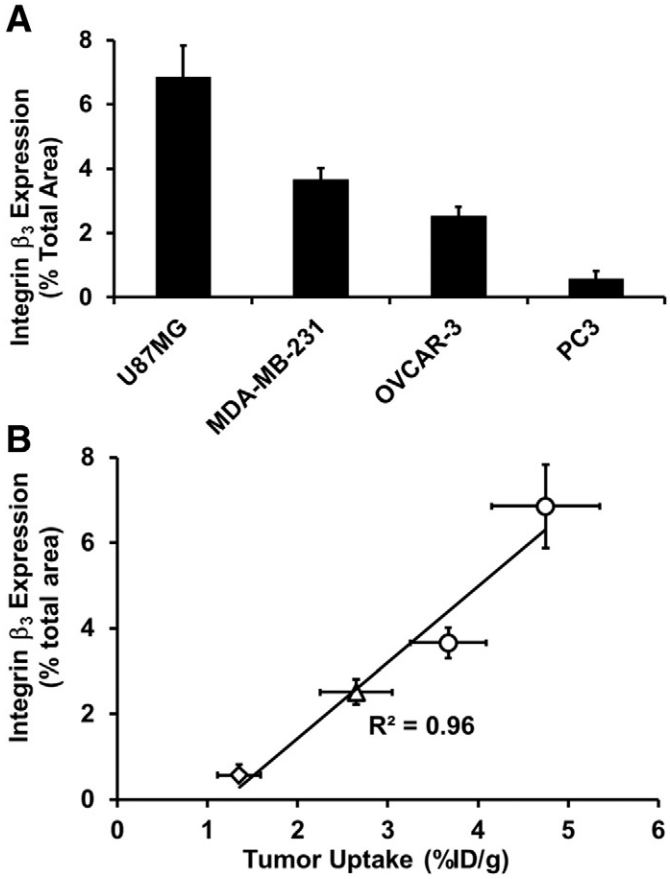

Fig. 5. A: Quantitative analysis of β_3 immunostaining from four different xenografted tumor tissues (U87MG, MDA-MB-231, OVCAR-3 and PC-3). The β_3 expression (tumor cells and neovasculature) was represented by the percentage of red area over the total area in each slice of tumor tissue. Each data point was derived from 10 different areas of the same tissue (200× magnification). Experiments were repeated three times independently with similar results. B: Linear relationship between the tumor uptake of ^{99m}Tc-I2P-RGD$_3$ from biodistribution (radioactivity density) and the relative β_3 expression levels (fluorescent density as represented by the % fluorescent intensity of red color over the total fluorescent intensity in the area) to illustrate the capability of ^{99m}Tc-I2P-RGD$_3$ to monitor the $\alpha_v\beta_3$ expression level in tumors of different origin.

images, the green color indicates the blood vessels, red color for the integrin β_3, and yellow color for the β_3 expressed on tumor vasculature. The $\alpha_v\beta_3$ expression follows the general ranking order of U87MG > MDA-MB-231 > OVAR-3 > PC-3, which is consistent with the tumor uptake data (Fig. 3B). Fig. 5A displays the quantitative data of β_3 for xenografted U87MG, MDA-MB-231, OVAR-3 and PC-3 tumor tissues. The β_3 level (fluorescence density) was defined by the percentage of red-colored area over the total area in each slice of tumor tissue. Since $\alpha_{IIB}\beta_3$ is expressed on activated platelets exclusively, the fluorescent intensity in tumor tissue is predominantly from the contribution of $\alpha_v\beta_3$. Fig. 5B displays plot of the tumor uptake (radioactivity density) of ^{99m}Tc-I2P-RGD$_2$ and $\alpha_v\beta_3$ expression levels (fluorescence density) in the U87MG, MDA-MB-231, OVAR-3 and PC-3 tumor tissues. There is a linear relationship between the %ID/g tumor uptake of ^{99m}Tc-I2P-RGD$_2$ and $\alpha_v\beta_3$ levels with R^2 being 0.9536.

4. Discussion

In this study, we use I2P-RGD$_2$ as the example to illustrate a novel approach for dimerization of cyclic RGD peptide. We found that the $\alpha_v\beta_3$ binding affinity of HYNIC-I2P-RGD$_2$ (Fig. 2: $IC_{50} = 39 \pm 6$ nM) was almost identical to that of HYNIC-3P-RGD$_2$ (Fig. 2: $IC_{50} = 32 \pm 5$ nM). Replacing glutamic acid with iminodiacetic acid has little impact on the $\alpha_v\beta_3$ binding affinity of dimeric cyclic RGD peptides, as long as the distance between two cyclic RGD moieties is long enough. This is also supported by the fact that ^{99m}Tc-I2P-RGD$_2$ and ^{99m}Tc-3P-RGD$_2$ shared almost identical tumor uptake over the 2 h period (Tables 1 and 2). The $\alpha_v\beta_3$ specificity of ^{99m}Tc-I2P-RGD$_2$ was demonstrated by the blocking experiment (Fig. 3B). There is a linear relationship between the %ID/g tumor uptake of ^{99m}Tc-I2P-RGD$_2$ and $\alpha_v\beta_3$ expression levels. SPECT data clearly show that ^{99m}Tc-I2P-RGD$_2$ is as good as ^{99m}Tc-3P-RGD$_2$ as a $\alpha_v\beta_3$-targeted radiotracer for tumor imaging. Therefore, iminodiacetic acid is an excellent bifunctional linker for dimerization and/or multimerization of cyclic RGD peptides.

In glutamic acid, the amino group is used for attachment of HYNIC (Fig. 1). In iminodiacetic acid, the secondary amine-N is used as the bridgehead. The 2-aminoethyl group is needed because it is difficult to conjugate HYNIC to secondary amine-N. As a result, ^{99m}Tc-I2P-RGD$_2$ and ^{99m}Tc-3P-RGD$_2$ display significant differences in their uptake in the intestines, kidneys and liver (Tables 1 and 2). ^{99m}Tc-I2P-RGD$_2$ had lower uptake than ^{99m}Tc-3P-RGD$_2$ in the kidneys and liver. In contrast, the uptake of ^{99m}Tc-I2P-RGD$_2$ was higher than those of ^{99m}Tc-3P-RGD$_2$ in the intestines. We reason that this difference might be related to the difference in their overall molecular charges. For 3P-RGD$_2$, the two positive charges on Arginine residues are neutralized by the two negatively charged carboxylate groups when the primary amino group is conjugated to HYNIC. For I2P-RGD$_2$, however, the secondary amine-N is likely protonated under physiological conditions (pH = 7.0–7.4). As a result, the overall molecular charge is most likely +1 for I2P-RGD$_2$.

Another important funding of this study is that there is a linear relationship (Fig. 5B) between the tumor uptake of ^{99m}Tc-I2P-RGD$_2$ (Table 1) and the relative $\alpha_v\beta_3$ expression levels (Fig. 5A), suggesting that ^{99m}Tc-I2P-RGD$_2$ is useful for monitoring the tumor $\alpha_v\beta_3$ expression in a noninvasive fashion. The capability to estimate the relative $\alpha_v\beta_3$ expression levels non-invasively is important for pre-treatment selection of the appropriate cancer patients who will benefit most from the anti-$\alpha_v\beta_3$ therapy. For example, if the tumor in a cancer patient has very high uptake of ^{99m}Tc-I2P-RGD$_2$, it would be most likely responsive to the anti-$\alpha_v\beta_3$ and antiangiogenesis treatment. Conversely, if the tumor in a cancer patient has little uptake of ^{99m}Tc-I2P-RGD$_2$, the anti-$\alpha_v\beta_3$ and antiangiogenesis therapy will not be effective regardless of the amount of drug administered to the cancer patient.

5. Conclusion

The results from this study clearly show that (1) iminodiacetic acid is as good as glutamic acid for dimerization of cyclic RGD peptides; (2) the bifunctional linkers (glutamic acid vs. iminodiacetic acid) have significant impact on the excretion kinetics of their corresponding ^{99m}Tc radiotracers; and (3) ^{99m}Tc-I2P-RGD$_2$ is an excellent radiotracer for tumor imaging. Because of its lower liver uptake and better tumor/liver ratios, ^{99m}Tc-I2P-RGD$_2$ may have advantages over ^{99m}Tc-3P-RGD$_2$ for diagnosis of tumors in chest region.

Conflict of interest

All authors declare that they have no conflict of interest.

Acknowledgment

This work was supported, in part, by Purdue University, the Indiana Clinical and Translational Sciences Institute funded in part by Grant No. TR000006 (Clinical and Translational Award) from the National Institutes of Health, the National Center for Advancing Translational Science, R21 EB017237-01 (S.L.) from the National Institute of Biomedical Imaging and Bioengineering (NIBIB), and Grants 81401446/81320108014 from the National Nature Science Foundation of China (YZ).

Appendix A Supplementary data

Radio-HPLC chromatograms of ^{99m}Tc-I2P-RGD$_2$ in the kit matrix at 1 and 6 h post-labeling (Fig. SI1) to demonstrate its solution stability, and representative microscopic fluorescent images of the xenografted U87MG, MDA-MB-231, OVCAR-3 and PC-3 tumor tissues (Fig. SI2) are all in word document. Supplementary data associated with this article can be found in the online version, at doi:10.1016/j.nucmedbio.2017.01.007.

References

[1] Lorger M, Krueger JS, O'Neal M, Staflin K, Felding-Habermann B. Activation of tumor cell integrin $\alpha_v\beta_3$ controls angiogenesis and metastatic growth in the brain. Proc Natl Acad Sci U S A 2009;106:10666–71.

[2] Omar O, Lennerås M, Svensson S, Suska F, Emanuelsson L, Hall J, et al. Integrin and chemokine receptor gene expression in implant-adherent cells during early osseointegration. J Mater Sci Mater Med 2010;21:969–80.

[3] Taherian A, Li X, Liu Y, Haas TA. Differences in integrin expression and signalling within human breast cancer cells. BMC Cancer 2011;11:293.

[4] Gupta A, Cao W, Chellaiah MA. Integrin $\alpha_v\beta_3$ and CD44 pathways in metastatic prostate cancer cells support osteoclastogenesis via a Runx2/Smad 5/receptor activator of NF-κB ligand signaling axis. Mol Cancer 2012;11:66.

[5] Vogetseder A, Thies S, Ingold B, Roth P, Weller M, Schraml P, et al. av-Integrin isoform expression in primary human tumors and brain metastases. Int J Cancer 2013;133:2362–71.

[6] Roth P, Silginer M, Goodman SL, Hasenbach K, Thies S, Maurer G, et al. Integrin control of the transforming growth factor-β pathway in glioblastoma. Brain 2013;136:564–76.

[7] Böger C, Kalthoff H, Goodman SL, Behrens HM, Röcken C. Integrins and their ligands are expressed in non-small cell lung cancer but not correlated with parameters of disease progression. Virchows Arch 2014;464:69–78.

[8] Zitzmann S, Ehemann V, Schwab M. Arginine–glycine–aspartic acid (RGD)-peptide binds to both tumor and tumor endothelial cells in vivo. Cancer Res 2002;62:5139–43.

[9] D'Andrea LD, Del Gatto A, Pedone C, Benedetti E. Peptide-based molecules in angiogenesis. Chem Biol Drug Des 2006;67:115–26.

[10] Meyer A, Auremheimer J, Modlinger A, Kessler H. Targeting RGD recognizing integrins: drug development, biomaterial research, tumor imaging and targeting. Curr Pharm Des 2006;12:2723–47.

[11] Liu S. Radiolabeled RGD peptides as integrin $\alpha_v\beta_3$-targeted radiotracers: maximizing binding affinity via bivalency. Bioconjug Chem 2009;20:2199–213.

[12] Stollman TH, Ruers TJM, Oyen WJG, Boerman OC. New targeted probes for radioimaging of angiogenesis. Methods 2009;48:188–92.

[13] Haubner R, Beer AJ, Wang H, Chen X. Positron emission tomography tracers for imaging angiogenesis. Eur J Nucl Med Mol Imaging 2010;37(Suppl. 1):S86–103.

[14] Dijkgraaf I, Boerman OC. Molecular imaging of angiogenesis with SPECT. Eur J Nucl Med Mol Imaging 2010;37(Suppl. 1):S104–13.

[15] Zhou Y, Chakraborty S, Liu S. Radiolabeled cyclic RGD peptides as radiotracers for imaging tumors and thrombosis by SPECT. Theranostics 2011;1:58–82.

[16] Beer AJ, Kessler H, Wester HJ, Schwaiger M. PET imaging of integrin $\alpha_v\beta_3$ expression. Theranostics 2011;1:48–57.

[17] Danhier F, Le Breton A, Préat V. RGD-based strategies to target $\alpha_v\beta_3$ integrin in cancer therapy and diagnosis. Mol Pharm 2012;9:2961–73.

[18] Tateishi U, Oka T, Inoue T. Radiolabeled RGD peptides as integrin $\alpha_v\beta_3$-targeted PET tracers. Curr Med Chem 2012;19:3301–9.

[19] Gaertner FC, Kessler H, Wester HJ, Schwaiger M, Beer AJ. Radiolabelled RGD peptides for imaging and therapy. Eur J Nucl Med Mol Imaging 2012;39(Suppl. 1):S126–38.

[20] Liu S. Radiolabeled cyclic RGD peptide conjugates as radiotracers targeting multiple integrins. Bioconjug Chem 2015;26:1413–38.

[21] Li ZB, Chen K, Chen X. ^{68}Ga-labeled multimeric RGD peptides for microPET imaging of integrin $\alpha_v\beta_3$ expression. Eur J Nucl Med Mol Imaging 2008;35:1100–8.

[22] Liu Z, Niu G, Shi J, Liu S, Wang F, Chen X. ^{68}Ga-labeled cyclic RGD dimers with Gly_3 and PEG_4 linkers: promising agents for tumor integrin $\alpha_v\beta_3$ PET imaging. Eur J Nucl Med Mol Imaging 2009;36:947–57.

[23] Liu Z, Liu S, Wang F, Chen X. Noninvasive imaging of tumor integrin expression using ^{18}F-labeled RGD dimer peptide with PEG_4 linkers. Eur J Nucl Med Mol Imaging 2009;36:1296–307.

[24] Shi J, Wang L, Kim YS, Zhai S, Liu Z, Chen X, et al. Improving tumor uptake and excretion kinetics of ^{99m}Tc-labeled cyclic arginine–glycine–aspartic (RGD) dimers with triglycine linkers. J Med Chem 2008;51:7980–90.

[25] Wang L, Shi J, Kim YS, Zhai S, Jia B, Zhao H, et al. Improving tumor targeting capability and pharmacokinetics of ^{99m}Tc-labeled cyclic RGD dimers with PEG_4 linkers. Mol Pharm 2009;6:231–45.

[26] Shi J, Wang L, Kim YS, Zhai S, Jia B, Wang F, et al. ^{99m}TcO(MAG_2-$3G_3$-dimer): a new integrin $\alpha_v\beta_3$-targeted radiotracer with high tumor uptake and favorable pharmacokinetics. Eur J Nucl Med Mol Imaging 2009;36:1874–84.

[27] Shi J, Kim YS, Zhai S, Liu Z, Chen X, Liu S. Improving tumor uptake and pharmacokinetics of ^{64}Cu-labeled cyclic RGD dimers with triglycine and PEG_4 linkers. Bioconjug Chem 2009;20:750–9.

[28] Shi J, Kim YS, Chakraborty S, Jia B, Wang F, Liu S. 2-Mercaptoacetylglycylglycyl (MAG_2) as a bifunctional chelator for ^{99m}Tc-labeling of cyclic RGD dimers: effects of technetium chelate on tumor uptake and pharmacokinetics. Bioconjug Chem 2009;20:1559–68.

[29] Chakraborty S, Kim YS, Shi J, Zhou Y, Wang F, Liu S. Evaluation of ^{111}In-labeled cyclic RGD peptides: tetrameric not tetravalent. Bioconjug Chem 2010;21:969–78.

[30] Zhou Y, Kim YS, Chakraborty S, Shi J, Gao H, Liu S. ^{99m}Tc-labeled cyclic RGD peptides for noninvasive monitoring of tumor integrin $\alpha_v\beta_3$ expression. Mol Imaging 2011;10:386–97.

[31] Shi J, Zhou Y, Chakraborty S, Kim YS, Jia B, Wang F, et al. Evaluation of ^{111}In-labeled cyclic RGD peptides: effects of peptide and PEG_4 multiplicity on their tumor uptake, excretion kinetics and metabolic stability. Theranostics 2011;1:322–40.

[32] Shi J, Jia B, Kim YS, Chakraborty S, Zhou Y, Wang F, et al. Impact of bifunctional chelators on biological properties of ^{111}In-labeled cyclic peptide RGD dimers. Amino Acids 2011;41:1059–70.

[33] Jacobson O, Zhu L, Niu G, Szajek L, Ma Y, Sun X, et al. MicroPET imaging of integrin $\alpha_v\beta_3$ expressing tumors using ^{89}Zr-RGD peptides. Mol Imaging Biol 2011;13:1224–33.

[34] Zhou Y, Kim YS, Lu X, Liu S. Evaluation of ^{99m}Tc-labeled cyclic RGD dimers: impact of cyclic RGD peptides and ^{99m}Tc chelates on biological properties. Bioconjug Chem 2012;23:586–95.

[35] Ji S, Zhou Y, Shao G, Liu S. Evaluation of K($HYNIC$)$_2$ as a bifunctional chelator for ^{99m}Tc-labeling of small biomolecules. Bioconjug Chem 2013;24:701–11.

[36] Ji S, Czerwinski A, Zhou Y, Shao G, Valenzuela F, Sowiński P, et al. ^{99m}Tc-Galacto-RGD_2: a ^{99m}Tc-labeled cyclic RGD peptide dimer useful for tumor imaging. Mol Pharm 2013;10:3304–14.

[37] Yang Y, Ji S, Liu S. Impact of multiple negative charges on blood clearance and biodistribution characteristics of ^{99m}Tc-labeled dimeric cyclic RGD peptides. Bioconjug Chem 2014;25:1720–9.

[38] Zheng Y, Ji S, Czerwinski A, Valenzuela F, Pennington M, Liu S. FITC-conjugated dimeric cyclic RGD peptides as fluorescent probes for in vitro assays of integrin $\alpha_v\beta_3$. Bioconjug Chem 2014;25:1925–41.

[39] Zheng Y, Ji S, Yang Y, Tomaselli E, Liu S. Comparison of biological properties of ^{111}In-labeled dimeric cyclic RGD peptides. Nucl Med Biol 2015;42:137–45.

[40] Zhao ZQ, Yang Y, Fang W, Liu S. Comparison of biological properties of ^{99m}Tc-labeled cyclic RGD peptide trimer and dimer useful as SPECT radiotracers for tumor imaging. Nucl Med Biol 2016;43:661–9.

[41] Ma Q, Ji B, Jia B, Gao S, Ji T, Wang X, et al. Differential diagnosis of solitary pulmonary nodules using ^{99m}Tc-3P-RGD scintigraphy. Eur J Nucl Med Mol Imaging 2011;38:2145–52.

[42] Zhu Z, Miao W, Li Q, Dai H, Ma Q, Wang F, et al. ^{99m}Tc-3PRGD2 for integrin receptor imaging of lung cancer: a multicenter study. J Nucl Med 2012;53:716–22.

[43] Zhao D, Jin X, Li F, Liang J, Lin Y. Integrin $\alpha_v\beta_3$ imaging of radioactive iodine–refractory thyroid cancer using ^{99m}Tc-3PRGD2. J Nucl Med 2012;53:1872–7.

[44] Ma Q, Chen B, Gao S, Ji T, Wen Q, Song Y, et al. ^{99m}Tc-3P4-RGD2 scintimammography in the assessment of breast lesions: comparative study with ^{99m}Tc-MIBI. PLoS One 2014;9:e108349.

[45] Liu L, Song Y, Gao S, Ji T, Zhan H, Ji B, et al. ^{99m}Tc-3PRGD2 scintimammography in palpable and nonpalpable breast lesions. Mol Imaging 2014;13:1–7.

[46] Wan W, Guo N, Pan D, Yu C, Weng Y, Luo S, et al. First experience of ^{18}F-Alfatide in lung cancer patients using a new lyophilized kit for rapid radiofluorination. J Nucl Med 2013;54:691–8.

[47] Guo J, Guo N, Lang L, Kiesewetter DO, Xie Q, Li Q, et al. ^{18}F-Alfatide II and ^{18}F-FDG dual-tracer dynamic PET for parametric, early prediction of tumor response to therapy. J Nucl Med 2014;55:154–60.

[48] Cheng W, Wu Z, Liang S, Fu H, Wu S, Tang Y, et al. Comparison of ^{18}F-AIF-NOTA-$PRGD_2$ and ^{18}F-FDG uptake in lymph node metastasis of differentiated thyroid cancer. PLoS One 2014;9:e100521.

[49] Yu C, Pan D, Mi B, Xu Y, Lang L, Niu G, et al. ^{18}F-Alfatide II PET/CT in healthy human volunteers and patients with brain metastases. Eur J Nucl Med Mol Imaging 2015;42:2021–8.

[50] Harris TD, Sworin M, Williams N, Rajopadhye M, Damphousse PR, Glowacka D, et al. Synthesis of stable hydrazones of a hydrazinonicotinyl-modified peptide for the preparation of ^{99m}Tc-labeled radiopharmaceuticals. Bioconjug Chem 1999;10:808–14.